

## 6.7: Long-range Electron Transfer in Proteins (Part 2)

### Cytochrome c

Cytochrome c occupies a prominent place in the mitochondrial electron-transport chain. Its water solubility, low molecular weight (12.4 kDa), stability, and ease of purification have allowed many experiments, which, when taken together, present a detailed picture of the structure and biological function of this electron carrier.<sup>128-133</sup>

X-ray structures<sup>134</sup> of oxidized and reduced tuna cytochrome c are very similar; most of the differences are confined to changes in the orientations of the side chains of some surface-exposed amino acids and sub-Ångström adjustments of some groups in the protein interior. Upon reduction, the heme active site becomes slightly more ordered (Figure 6.33). Two-dimensional NMR studies<sup>135-137</sup> confirm this interpretation of the x-ray data, and further establish that the crystal and solution structures of cytochrome c differ in only minor respects.

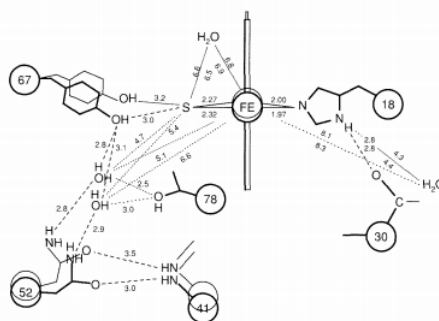


Figure 6.33: Side-chain motion in the vicinity of the heme of cytochrome c. Heavy lines indicate the reduced molecule, and light lines the oxidized molecule.<sup>134</sup>

Cytochrome c exhibits several pH-dependent conformational states. In particular, an alkaline transition with a  $pK_a \sim 9.1$  has been observed for ferricytochrome c. This transition is believed to be associated with the dissociation of Met-80; the reduction potential decreases dramatically,<sup>138</sup> and the 695-nm absorption band, associated with a sulfur  $\rightarrow$  iron charge-transfer transition, disappears. The  $^2\text{H}$  NMR resonance due to ( $^2\text{H}_3\text{C}$ -) Met-80 in deuterium-enriched ferricytochrome c disappears from its hyperfine-shifted upfield position without line broadening, and reappears coincident with the ( $^2\text{H}_3\text{C}$ -)Met-65 resonance.<sup>139</sup> In contrast, ferrocyanochrome c maintains an ordered structure over the pH range 4 to 11.<sup>140</sup> The heme iron in ferricytochrome c remains low-spin throughout this transition, and a new strong-field ligand must therefore replace Met-80. It has been suggested that an  $\epsilon$ -amino nitrogen of a nearby Lys provides the new donor atom, but this has not been confirmed. However, it is clear that reduction of ferricytochrome c at alkaline pH values below 11 causes a drastic conformational change at the heme site. The unknown sixth ligand must be displaced by Met-80 in order for the reduced protein to assume a structure similar to the one at neutral pH. This structural change is accompanied by a decrease in the rate of reduction of ferricytochrome c by hydrated electrons,<sup>141</sup> as expected.

How does the protein control the reduction potential of the iron center in cytochrome c? Factors that appear to play a role include the nature of the axial ligands, the stability and solvent accessibility of the heme crevice, and the hydrophobicities of the amino acids that line the heme crevice. These issues have been addressed theoretically<sup>142,143</sup> and experimentally<sup>144-149</sup> using cytochrome c variants engineered by protein semisynthesis or site-directed mutagenesis. Results for horse heart cytochrome c are set out in Table 6.6. Point mutations at either of positions 78 or 83 do not significantly alter  $E^\circ$ ; however, the double mutant (Thr-78  $\rightarrow$  Asn-78; Tyr-83  $\rightarrow$  Phe-83) exhibits a substantially lower redox potential. Evidently, the results of such changes are not necessarily additive; great care must be taken in drawing conclusions about structure-function relations in engineered proteins. Finally, the  $\sim 310$  mV difference between the values for the heme octapeptide and the native protein (the axial ligands are the same in both) provides a dramatic illustration of protein environmental effects on the redox potential: shielding the heme from the solvent is expected to stabilize  $\text{Fe}^{\text{II}}$  and therefore result in an increase in  $E^\circ$ .

Table 6.6: Reduction potentials of horse heart cytochrome c. a) pH 7.0, 25 °C. b) In 2M N-acetyl-DL-methionine.

Cytochrome	$E^\circ$ (mV vs. NHE)	Reference
Native	262	138
Met-80 $\rightarrow$ His-80	41	144

Cytochrome	$E^{\circ}$ (mV vs. NHE)	Reference
Tyr-67 → Phe-67	225	145
Thr-78 → Asn-78	264	145
Tyr-83 → Pro-83	266	145
Thr-78, Tyr-83 → Asn-78, Pro-83	235	145
Heme octapeptide <sup>b</sup>	-50	146

During the last fifteen years, much has been learned about the interaction of cytochrome *c* with its redox partners.<sup>128-133</sup> Cytochrome *c* is a highly basic protein ( $pI = 10.05$ ); lysine residues constitute most of the cationic amino acids. Despite the indication from the x-ray structures that only ~1 percent of the heme surface is solvent-exposed, the asymmetric distribution of surface charges, particularly a highly conserved ring of Lys residues surrounding the exposed edge of the heme crevice, led to the suggestion that electron-transfer reactions of cytochrome *c* (and other Class I cytochromes as well) occur via the exposed heme edge.

Chemical modification of the surface Lys residues of cytochrome *c* has afforded opportunities to alter the properties of the surface  $\epsilon$ -amino groups suspected to be involved in precursor complex formation. Margoliash and coworkers<sup>133,150,151</sup> used a 4-carboxy-2,6-dinitrophenol (CDNP) modification of the Lys residues to map out the cytochrome *c* interaction domains with various transition-metal redox reagents and proteins. These experiments have shown that cytochrome *c* interacts with inorganic redox partners near the exposed heme edge.

Numerous studies<sup>129,152,153</sup> of cytochrome *c* with physiological reaction partners are in accord with electrostatic interactions featured in the model cytochrome *c*/cytochrome  $b_5$  complex discussed earlier. Similar types of interactions have been proposed for cytochrome *c*/flavodoxin<sup>154</sup> and cytochrome *c*/cytochrome *c* peroxidase complexes.<sup>155</sup> (Recent x-ray crystal structure work<sup>155b</sup> has shed new light on this problem.) Theoretical work<sup>156</sup> additionally suggests that electrostatic forces exert torques on diffusing protein reactants that "steer" the proteins into a favorable docking geometry. However, the domains on cytochrome *c* for interaction with physiological redox partners are not identical, as Figure 6.34 illustrates.

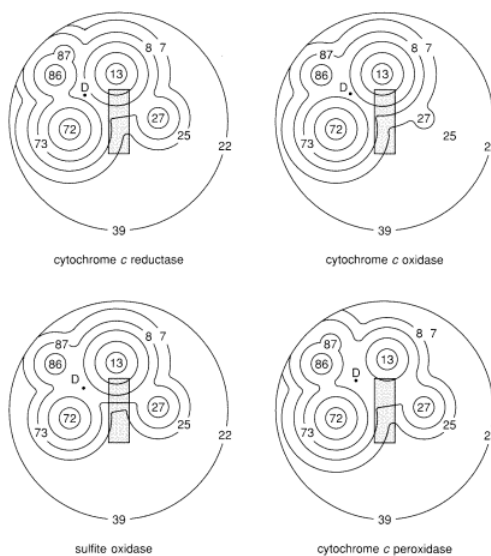


Figure 6.34: Domains on cytochrome *c* for interaction with physiological redox partners. The heme edge is represented by the shaded rectangle. The number of circles around a given Lys residue is proportional to the percentage of the observed inhibition in redox assays when the corresponding CDNP-modified cytochrome *c* is used.<sup>151</sup>

Reactions between cytochrome *c* and its physiological redox partners at low ionic strength generally are very fast,  $\sim 10^8 \text{ M}^{-1}\text{s}^{-1}$ , even though the thermodynamic driving force may be as low as 20 mV, as it is for the reduction of cytochrome *a* in cytochrome *c* oxidase. Such rates are probably at the diffusion-controlled limit for such protein-protein reactions.<sup>157,158</sup> A more detailed understanding of these reactions will require studies that focus on the dynamical (rather than static) features of complexes of cytochrome *c* with other proteins. For example, there is evidence<sup>159</sup> that a cytochrome *c* conformational change in the vicinity of

the heme edge accompanies the formation of the complex with cytochrome c oxidase. Studies of the influence of geometry changes on activation energies<sup>52,60,160</sup> are of particular importance in elucidating the mechanisms of protein-protein reactions.

### 1. Ruthenium-modified Cytochrome c

Intramolecular electron transfer in cytochrome c has been investigated by attaching photoactive Ru complexes to the protein surface.<sup>98,161</sup> Ru(bpy)<sub>2</sub>(CO<sub>3</sub>) (bpy = 2,2'-bipyridine) has been shown to react with surface His residues to yield, after addition of excess imidazole (im), Ru(bpy)<sub>2</sub>(im)(His)<sup>2+</sup>. The protein-bound Ru complexes are luminescent, but the excited states (\*Ru<sup>2+</sup>) are rather short lived ( $\tau \leq 100$  ns). When direct electron transfer from \*Ru<sup>2+</sup> to the heme cannot compete with excited-state decay, electron-transfer quenchers (e.g., Ru(NH<sub>3</sub>)<sub>6</sub><sup>3+</sup>) are added to the solution to intercept a small fraction (1-10%) of the excited molecules, yielding (with oxidative quenchers) Ru<sup>3+</sup>. If, before laser excitation of the Ru site, the heme is reduced, then the Fe<sup>2+</sup> to Ru<sup>3+</sup> reaction ( $k_{et}$ ) can be monitored by transient absorption spectroscopy. The  $k_{et}$  values for five different modified cytochromes have been reported: (Ru(His-33), 2.6(3) x 10<sup>6</sup>; Ru(His-39), 3.2(4) x 10<sup>6</sup>; Ru(His-62), 1.0(2) x 10<sup>4</sup>; Ru(His-72), 9.0(3) x 10<sup>5</sup>; and Ru(His-79), > 10<sup>8</sup> s<sup>-1</sup>).<sup>162,163</sup>

According to Equation (6.27), rates become activationless when the reaction driving force ( $-\Delta G^\circ$ ) equals the reorganization energy (A). The driving force (0.74 eV) is approximately equal to the reorganization energy (0.8 eV) estimated for the Ru(bpy)<sub>2</sub>(im)(His)-cyt c reactions.<sup>161</sup> The activationless (maximum) rates ( $k_{max}$ ) are limited by  $H_{AB}^2$ , where  $H_{AB}$  is the electronic matrix element that couples the reactants and products at the transition state. Values of  $k_{max}$  and  $H_{AB}$  for the Fe<sup>2+</sup> to Ru<sup>3+</sup> reactions are given in Table 6.7.

Table 6.7: Electron-transfer parameters<sup>163</sup> for Ru(bpy)<sub>2</sub>(im)(His-X)-cytochromes c.a) C = covalent bond, H = hydrogen bond, S = space jump.

X	$k_{max}$ (s <sup>-1</sup> )	$H_{AB}$ (cm <sup>-1</sup> ) [Fe <sup>2+</sup> — Ru <sup>3+</sup> ]	$d$ (Å)	$n_{eff}^a$	$\sigma$ 1(Å)
79	> 1.0 x 10 <sup>8</sup>	> 0.6	4.5	8 (8C)	11.2
39	3.3 x 10 <sup>6</sup>	0.11	12.3	14.0 (11C) (1H)	19.6
33	2.7 x 10 <sup>6</sup>	0.097	11.1	13.9 (11C) (1H)	19.5
72	9.4 x 10 <sup>5</sup>	0.057	8.4	17.6 (7C) (1S)	24.6
62	1.0 x 10 <sup>4</sup>	0.006	14.8	20.6 (16C) (2H)	28.8

Calculations that explicitly include the structure of the intervening medium<sup>81-86,164-169</sup> have been particularly helpful in developing an understanding of distant electronic couplings. As discussed in Section IV.A, the couplings in proteins can be interpreted in terms of pathways comprised of covalent, H-bond, and through-space contacts. An algorithm has been developed<sup>85,170</sup> that searches a protein structure for the best pathways coupling two redox sites (the pathways between the histidines (33, 39, 62, 72, 79) and the heme are shown in Figure 6.35). A given coupling pathway consisting of covalent bonds, H-bonds, and through-space jumps can be described in terms of an equivalent covalent pathway with an effective number of covalent bonds ( $n_{eff}$ ). Multiplying the effective number of bonds by 1.4 Å/bond gives a-tunneling lengths ( $\sigma$ ) for the five pathways (Table 6.7) that correlate well with the maximum rates (one-bond limit set at 3 x 10<sup>12</sup> s<sup>-1</sup>; slope of 0.71 Å<sup>-1</sup>) (Figure 6.35). The 0.71 Å<sup>-1</sup> decay accords closely with related distance dependences for covalently coupled donor-acceptor molecules.<sup>73,77</sup>

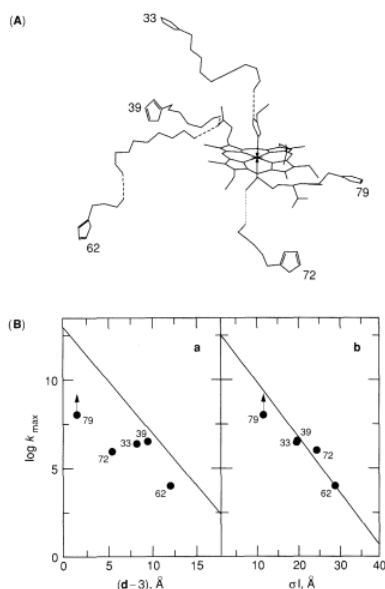


Figure 6.35 - (A) Electronic coupling pathways to the heme from Ru-modified residues in native (His-33 horse heart, His-39 yeast), genetically engineered (His-62 yeast), and semisynthetic (His-72, His-79 horse heart) cytochromes c. Solid lines are covalent bonds; dashed lines are hydrogen bonds; and the dotted line (His-72 pathway) is a space jump. (B) The left half of the diagram (a) shows maximum electron-transfer rate vs.  $d$  minus 3 Å (van der Waals contact). Exponential-decay line with  $1 \times 10^{13} \text{ s}^{-1}$  intercept and  $1.4 \text{ Å}^{-1}$  slope. The right half of the diagram (b) shows maximum rate vs.  $\sigma_1$ :  $0.71 \text{ Å}^{-1}$  slope;  $3 \times 10^{12} \text{ s}^{-1}$  intercept. Adapted from References 162 and 163.

## Bacterial Photosynthetic Reaction Centers

Photosynthetic bacteria produce only one type of reaction center, unlike green plants (which produce two different kinds linked together in series), and are therefore the organisms of choice in photosynthetic electron-transfer research.<sup>171-176</sup> As indicated in Section I.B, the original reaction center structure (Figure 6.15) lacked a quinone ( $Q_B$ ). Subsequent structures for reaction centers from other photosynthetic bacteria<sup>177,178</sup> contain this quinone (Figure 6.36 See color plate section, page C-13.). The *Rps. sphaeroides* reaction center contains ten cofactors and three protein subunits. (Note that the *Rps. viridis* structure contains a cytochrome subunit as well.) The cofactors are arrayed so that they nearly span the 40-Å-thick membrane (Figure 6.37 See color plate section, page C-13.). The iron atom is indicated by the red dot near the cytoplasmic side of the membrane (bottom). In spite of the near two-fold axis of symmetry, electron transfer proceeds along a pathway that is determined by the A branch. In particular,  $BChl_B$  and  $BPhe_B$  do not appear to play an important role in the electron transfers.

It was demonstrated long ago that  $(BChl)_2$  is the primary electron donor and that ubiquinone (or metaquinone) is the ultimate electron acceptor. Transient flash photolysis experiments indicate that several electron-transfer steps occur in order to translocate the charge across the membrane (Figure 6.38). Curiously, the high-spin ferrous iron appears to play no functional role in the  $Q_A$  to  $Q_B$  electron transfer.<sup>179</sup> In addition, the part played by  $BChl_A$  is not understood—it may act to promote reduction of  $BPhe_A$  via a superexchange mechanism.<sup>180,181</sup> Cytochromes supply the reducing equivalents to reduce the special pair  $(BChl)_2^+$ .

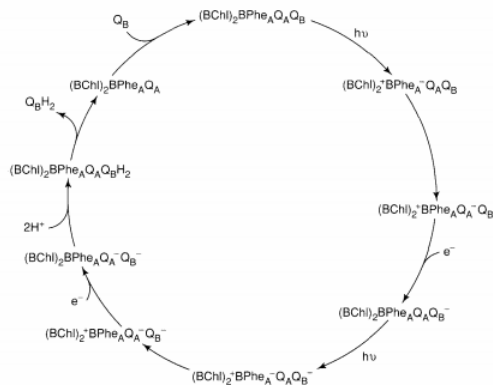


Figure 6.38 - Forward electron transfer through the reaction center. Note that two charge translocations must occur in order for the (labile) quinol  $Q_BH_2$  to be produced. Once  $Q_BH_2$  dissociates from the RC and is replaced by another, oxidized,  $Q_B$ , the cycle can begin anew.

Estimated rate constants for the various electron-transfer steps, together with approximate reduction potentials, are displayed in Figure 6.39. For each step, the forward rate is orders of magnitude faster than the reverse reaction. The rapid rates suggest that attempts to obtain x-ray structures of intermediates (especially the early ones!) will not be successful. However, molecular dynamics methods are being explored in computer simulations of the structures of various intermediates.<sup>182,183</sup> Within a few years we may begin to understand why the initial steps are so fast.

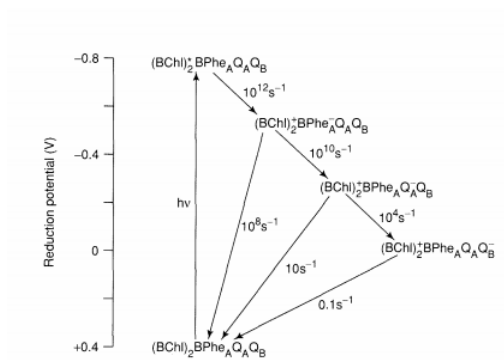


Figure 6.39 - Electron-transfer rates (for forward and reverse reactions) and reduction potentials for RC intermediates.

6.7: Long-range Electron Transfer in Proteins (Part 2) is shared under a [CC BY-NC-SA 4.0](https://creativecommons.org/licenses/by-nc-sa/4.0/) license and was authored, remixed, and/or curated by LibreTexts.